Structural Engineering and Mechanics, *Vol. 71, No. 6 (2019) 683-697*
DOI: https://doi.org/10.12989/sem.2019.71.6.683

Application of an extended Bouc-Wen model for hysteretic behavior of the RC structure with SCEBs

Huihui Dong[1,2a], Qiang Han*[1] and Xiuli Du[1b]

[1]*Key Laboratory of Urban Security and Disaster Engineering of Ministry of Education, Beijing University of Technology, Beijing 100124, China*
[2]*Key Laboratory of Civil Engineering Safety and Durability of China Education Ministry, Department of Civil Engineering, Tsinghua University, Beijing 100084, China*

(Received December 26, 2018, Revised April 1, 2019, Accepted April 9, 2019)

Abstract. The reinforced concrete (RC) structures usually suffer large residual displacements under strong motions. The large residual displacements may substantially reduce the anti-seismic capacity of structures during the aftershock and increase the difficulty and cost of structural repair after an earthquake. To reduce the adverse residual displacement, several self-centering energy dissipation braces (SCEBs) have been proposed to be installed to the RC structures. To investigate the seismic responses of the RC structures with SCEBs under the earthquake excitation, an extended Bouc-Wen model with degradation and self-centering effects is developed in this study. The extended model realized by MATLAB/Simulink program is able to capture the hysteretic characteristics of the RC structures with SCEBs, such as the energy dissipation and the degradation, especially the self-centering effect. The predicted hysteretic behavior of the RC structures with SCEBs based on the extended model, which used the unscented Kalman filter (UKF) for parameter identification, is compared with the experimental results. Comparison results show that the predicted hysteretic curves can be in good agreement with the experimental results. The nonlinear dynamic analyses using the extended model are then carried out to explore the seismic performance of the RC structures with SCEBs. The analysis results demonstrate that the SCEB can effectively reduce the residual displacements of the RC structures, but slightly increase the acceleration.

Keywords: Bouc-Wen model; self-centering energy dissipation brace; RC structure: seismic response analysis; self-centering effect

1. Introduction

The conventional seismic structures designed and constructed according to the current seismic design codes can avoid structural collapse during weak or moderate earthquakes, while they may be in the inelastic state that results in large residual deformations after strong earthquakes. The extent of the residual deformation is one of the crucial factors determining the structural safety and the structural repair cost after earthquakes. Therefore, it is required to develop a self-centering structural system for eliminating the residual deformation of the structure (McCormick *et al*. 2008, Erochko *et al*. 2010). The self-centering structures behave the self-centering capability that can return the structure to its initial position after earthquakes. At present, various self-centering structures have been proposed and verified by experimental and numerical studies (Christopoulos *et al*. 2002, Ricles *et al*. 2002, Ajrab *et al*. 2004, Chou and Lai 2009, Kim and Christopoulos 2009, Ma *et al*. 2010, Nicknam and Filiatrault 201, Rahgozar *et al*. 2017, Li and Qiu 2018, Li *et al*. 2018, Han *et al*. 2019). Among these self-centering structures, the self-centering energy dissipation braced (SCEB) structures have been widely applied, because the installation and replacement of the braces are relatively easy and convenient.

At present, types of SCEBs have been proposed (Dolce *et al*. 2000, Zhu and Zhang 2007, Li *et al*. 2008, Ma and Cho 2008, Tremblay *et al*. 2008, Miller *et al*. 2012, Zhou *et al*. 2015, Xu *et al*. 2016, Xu *et al*. 2017). These proposed SCEBs normally include an energy dissipation group and a self-centering group. They can provide a stable energy dissipation capability and the large restoring force to the primary structure to enable the whole system to have the re-centering capability. For example, Zhu and Zhang (Zhu and Zhang 2007, Zhu and Zhang 2008) proposed an SCEB based on SMA and experimentally investigated its hysteretic behaviour. The numerical simulation results of the seismic responses on the steel frame with the SCEB based on SMA showed the braced frame can obviously eliminate the residual drift ratio. A novel SCEB using the composite tensioning elements was developed and investigated by Christopoulos and Tremblay (Christopoulos *et al*. 2008, Tremblay *et al*. 2008, Tremblay and Christopoulos 2012), and quasi-static and dynamic validation tests of the full-scale steel frame with this SCEB were performed. These experimental results demonstrated

*Corresponding author, Professor
E-mail: qhan@bjut.edu.cn
[a] Ph.D.
E-mail: donghuihui.123@163.com
[b] Professor
E-mail: xiulidu1@126.com

ISSN: 1225-4568 (Print), 1598-6217 (Online)

that the SCEB and the steel frame with SCEB under quasi-static and dynamic loadings both behave the stable energy dissipation ability and excellent self-centering capability. Ozbulut and Hurlebaus (Ozbulut *et al*. 2011, Ozbulut and Hurlebaus 2012) presented a new SCEB combined energy dissipation capabilities of a variable friction damper with the re-centering ability of SMA, and investigated the seismic responses of a 20-story nonlinear benchmark building with the new SCEB. Araki *et al*. (2016) performed shaking table tests of a one-bay one-story steel frame with SCEB. The test results demonstrated that the SCEB can effectively prevent residual deformations and pinching of the structures. Xu *et al*. (Xu *et al*. 2016, Xu, Fan and Li 2017) developed a pre-pressed spring self-centering energy dissipation devices with pre-pressed disc springs. Some SCEBs combined the pre-tensile tendon elements with buckling restrained brace were also recently developed (Miller *et al*. 2011, Chou and Chen 2012, Zhou *et al.* 2015, Dong *et al*. 2017, 2019). Most previous research studies mainly focused on the hysteretic behavior of the SCEB and the seismic responses of the steel frames with SCEBs. It should be noted that the mathematical hysteretic model and its parameter identification of such structure are the key parts for the seismic response analyses.

To date, some mathematical models have been proposed to describe some complex nonlinear hysteresis characteristics of the common steel and RC structures. These proposed models can be typically classified into two types according to the smoothness of hysteretic loop (Clough *et al*. 1965, Takeda *et al*. 1970, Saiidi and Sozen 1981, Sivaselvan and Reinhorn 2000): polygonal hysteretic models and smooth hysteretic models. The previous literature review reveals (Zhu and Zhang 2007, Tremblay *et al*. 2008, Zhu and Zhang 2008, Zhu and Zhang 2008, Erochko *et al*. 2010, Ozbulut and Hurlebaus 2012, Chou and Chung 2014, Eatherton *et al*. 2014, Eatherton *et al*. 2014, Erochko *et al*. 2014, Araki *et al*. 2016) that these proposed SCEBs and the frame with SCEB both behave a typical flag-shape hysteretic behavior with stable energy dissipation capability and excellent self-centering ability, and the frame structures with SCEBs show small residual displacement. So far, some hysteretic models have been applied to the self-centering structure. For example, Ma *et al*. (2011) developed the hysteretic model of the SMA damper by using the initial Bouc-Wen model to describe the energy dissipating capacity and using the rigid-elastic model to represent the re-centering ability, and the model was applied to investigate the seismic performance of the steel frames with the SMA dampers. Kitayama *et al*. (Kitayama and Constantinou 2016, Kitayama and Constantinou 2017) used a mathematical model based on Bouc-Wen model to simulate the hysteretic behavior of the fluidic self-centering systems, and the results showed that the predicted hysteretic curves based on the mathematical model can be in good agreement with the experimental results. An extended Bouc-Wen model with the pinched hysteresis behavior was used to predict the nonlinear response of the SMA cables (Carboni *et al*. 2014). Xu *et al*. (2016) adopted the piecewise function based on the Bouc-Wen model to predict the hysteresis response of the SCEB. Moreover, Huang *et al*. (2002) suggested using a cyclic elastoplastic model based on the rheological analysis method to investigate the hysteretic model of the SCEB. It should be noted that the above studies were focused on the hysteretic models of the various SCEBs and the steel structure with SCEBs, no literature reports the elastoplastic smooth model and its parameter identification for the RC structures with SCEBs yet.

The Bouc-Wen model is one of the most popular smooth hysteretic models, introduced by Bouc (1967) and later extended by Wen and Baber (Wen 1976, Baber and Wen 1981, Baber and Noori 1985), which could represent a wide variety of softening or hardening smoothly varying hysteretic behavior. With the great development of computational efficiency and accuracy, the Bouc-Wen model has been widely employed in the field of the structural engineering (Sireteanu *et al*. 2010, Domaneschi 2012, Chang *et al*. 2016). Therefore, the focus of this study is to propose an extended Bouc-Wen model for predicting the seismic performance of the RC structure with SCEBs. The extended model is capable of capturing the primary hysteretic behaviors of the RC structure with SCEBs such as the self-centering effect, strength and stiffness degradations. The predicted hysteretic behaviors of the RC structures with SCEBs based on the extended Bouc-Wen model are achieved by programming in the Matlab/Simulink environment, and the UKF is used for the parameter identification. To examine the accuracy of the extended model, the predicted hysteretic curves of the RC structure with SCEBs based on the extended model under quasi-static load are simulated and compared with the experimental results. Furthermore, the nonlinear dynamic analyses based on the extended model are conducted to explore the seismic performance of the RC structures with SECBs subject to earthquake excitations.

2. RC structure with SCEB

Fig. 1 shows the concept of SCEB. As shown, a traditional SCEB normally consists of two systems, the pre-tensioned tendons/pre-pressed springs as the self-centering system and the friction/viscous/yielding device acting as the energy dissipation system. Alternatively, the energy dissipation system can be omitted from the system, and the energy dissipation can be provided by specialized tensioning elements such as SMA. In SCEB, structural members and blocking plates are also necessary as the members, and the blocking plates act as not only stopper but also connection plates. The energy dissipation system is connected to the two structural members and is activated when the two structural members occur the relative motions. The pre-tensioned tendons/pre-pressed springs are installed on the two structural members, and their geometric properties can be selected to achieve the desired strength, post-yielding stiffness, deformation capacity and the self-centering capacity of the self-centering system. In the self-centering system, the force of the pre-tension/pre-pressed in the tendons/springs determines the activating force at which the relative movement starts between the two structural

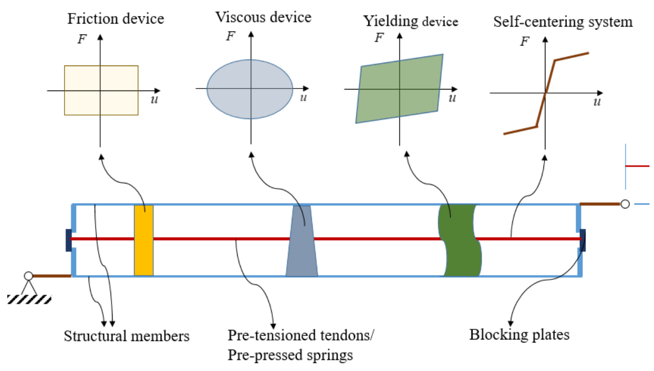

Fig. 1 Concept of SCEB

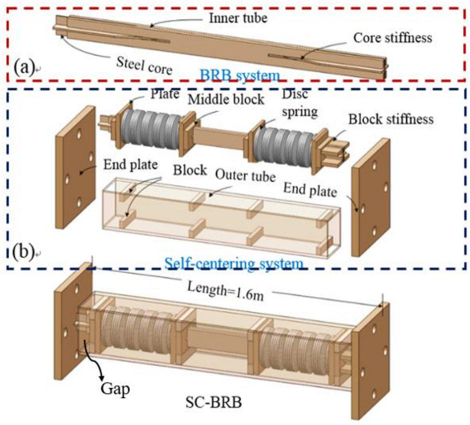

Fig. 2 Schematic drawing of the SCEB

members. The force of the pre-tension/pre-pressed also controls the self-centering capability of the SCEB: full self-centering behavior can be achieved when the pre-tension/ pre-pressed force is larger than or equal to the force of the energy dissipation system.

Although the traditional SCEB described in the previous paragraph consists of the pre-tension tendons/pre-pressed springs and the friction/viscous/yield device, one embodiment SCEB is illustrated in Fig. 2 and studied in more detail in the following sections. This SCEB consists of a traditional buckling restrained brace (BRB) group and a self-centering group as shown in Fig. 2 (Dong *et al*. 2017). In this SCEB system, the steel core, the rectangular inner steel tube and the end plates form the traditional BRB system as shown in Fig. 2(a). The self-centering system is composed of two groups of disc springs, the square outer steel tube, as shown in Fig. 2(b).

The SCEB is installed to the RC structure to improve its seismic performance. The schematic drawing of the RC structure with SCEB is shown in Fig. 3(a). As shown, the RC structure with SCEB can be regarded as the RC structure system and the SCEB system assembled in parallel. Fig. 3(b) presents the mass-spring-dashpot idealization of the RC structure with SCEB. In Fig. 3(b), F_s, F_b and F_R are the forces of the self-centering system, the BRB system and the RC structure, respectively. Because of the RC structure system and the SCEB system assembled in parallel, the deformations of the RC structure and the SCEB are the same, and the force of the RC structure with SCEB is the summation of those provided by the RC structure and the SCEB systems, as shown in Fig. 3(b).

Fig. 3(c) shows the hysteretic behavior of the RC structure with SCEB. The hysteresis response of the SCEB is equal to the summation of those of the self-centering and the BRB systems

$$k_{SCEB1} = k_{s1} + k_{b1} \tag{1}$$

$$k_{SCEB2} = k_{s2} + k_{b2} \tag{2}$$

$$f_{SCEBy} = f_{sy} + f_{by} \tag{3}$$

where, k_{SCEB1}, k_{s1} and k_{b1} are the initial stiffness of the SCEB, the self-centering system and the BRB, k_{SCEB2}, k_{s2} and k_{b2} are the post-yielding stiffness of the SCEB, the self-centering system and the BRB, f_{SCEBy}, f_{sy} and f_{by} are the yield force of the SCEB, the self-centering system and the BRB.

For the RC structure with SCEB, the total hysteresis behavior is equal to the total of those of the SCEB and RC structure systems

$$k_{RC-S1} = k_{SCEB1} + k_{R1} \tag{4}$$

$$k_{RC-S2} = k_{SCEB2} + k_{R2} \tag{5}$$

$$f_{RC-Sy} = f_{SCEBy} + f_{Ry} \tag{6}$$

where, k_{RC-S1} and k_{R1} are the initial stiffness of the RC structure with SCEB and the SCEB, k_{RC-S2} and k_{R2} are the post-yield stiffness of the RC structure with SCEB and the SCEB, f_{RC-Sy} and f_{Ry} are the yield force of the RC structure with SCEB and the SCEB.

The hysteretic curves of the RC structure with SCEB behave the typical flag shape with the self-centering ability and the energy dissipation capability as shown in Fig. 3(c). This result coincides well with some of previous investigations (e.g. (Zhu and Zhang 2008, Chou and Chung 2014, Erochko *et al*.2014, Zhou, Xie *et al*. 2015, Xu *et al*. 2016)). Moreover, it should be noted that the hysteretic curves of the RC structure without brace normally show obvious degradation and pinching effects due to the severe damages at the concrete and rebar (Elbahey and Bruneau 2012, Bazaez and Dusicka 2016).

3. Proposed analytical hysteresis model

3.1 Classical Bouc-Wen Model

The equation of the motion of the single degree of freedom (SDOF) is expressed as

$$m\ddot{x}(t) + c\dot{x}(t) + F(t) = f(t) \tag{7}$$

where m is the mass of the system, c is the structure system inherently linear viscous damping, $\dot{x}$ and $\ddot{x}$ are the system velocity and acceleration respectively, $F(t)$ is the restoring force, $f(t)$ is the earthquake excitation force.

The restoring force $F(t)$ based on Bouc-Wen model is given by

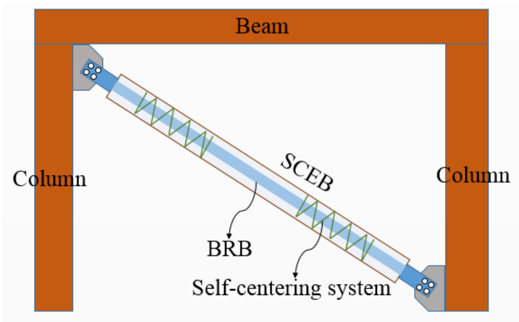

(a) schematic drawing

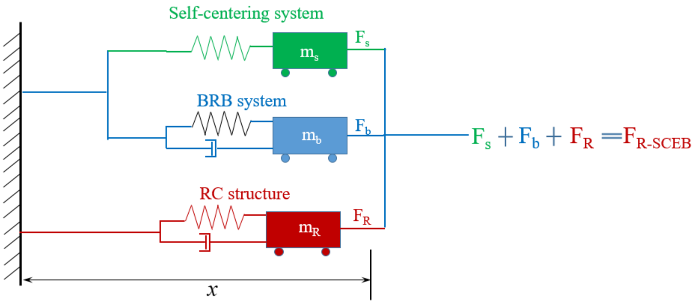

(b) mass-spring-dashpot idealization

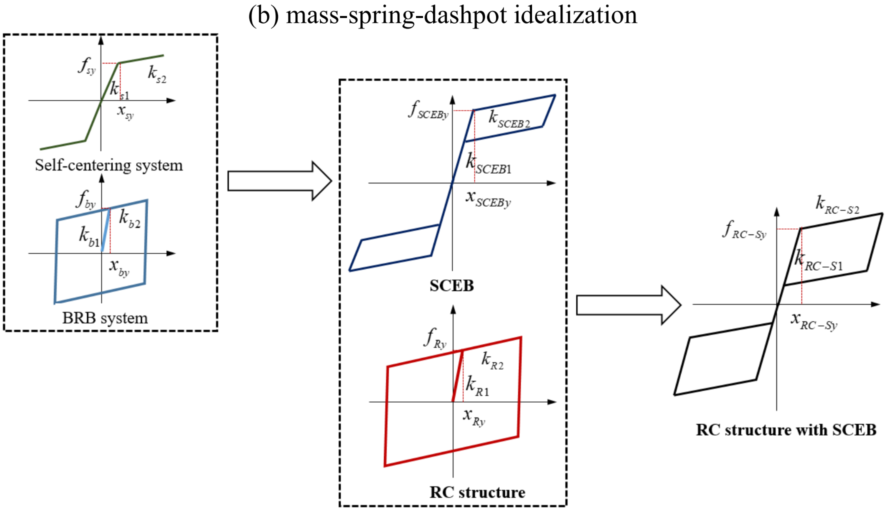

(c) hysteretic curve

Fig. 3 RC structure with SCEB

$$F(t) = ak_1x(t) + (1-a)k_1z(t) \tag{8}$$

where k_1 is the initial stiffness of the system, a is the ratio of the post-yield stiffness to the pre-yielding stiffness, z is the hysteresis displacement. The properties of z depend on the material and structural properties, the derivative of the hysteresis displacement z can be obtained by

$$\dot{z} = \dot{u} - \beta|\dot{x} \cdot z|z^{n-1} - \gamma \cdot \dot{x} \cdot z^n \tag{9}$$

where β is the parameter of the shape controlling, γ is the parameter for controlling the loop size, n is the parameter for controlling the loop smoothness (when n is small, the transition from pre-yielding to post-yielding is smooth, while the transition becomes abrupt for the large value of n, approaching that of a bilinear model). Moreover, the values of β and n should be positive, while γ can be either positive or negative (Foliente 1995).

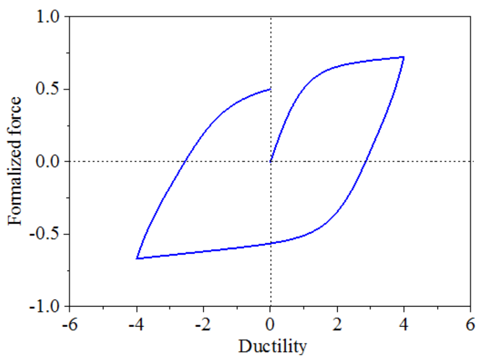

Fig. 4 Hysteresis curve of the initial Bouc-Wen model

Fig. 4 shows the dimensionless hysteresis curves based on the initial Bouc-Wen model. In this figure, the ductility is the ratio of the ultimate displacement divided by the yield displacement. It can be seen from Fig. 4 that the stiffness change of the hysteretic curves based on the initial Bouc-Wen model is continuous and smooth.

The inelastic response of the RC structures under earthquakes may be accompanied by stiffness degradation, strength degradation and pinching effects as previous studies mentioned (Elbahey and Bruneau 2012, Bazaez and Dusicka 2016), because of that, the hysteretic model is required to consider the degradation and pinching effects. Therefore, two new functions for the initial Bouc-Wen model were introduced by Baber and Wen (1981), which can respectively describe the strength degradation and the stiffness degradation of the RC structure. Baber and Noori (1985) further extended this hysteretic model considering the pinching effect, the extended model used the smooth hysteretic element in series with a time-dependent slip-lock element.

The extended Bouc-Wen model considering the degradation and pinching effects can be expressed as follows

$$\dot{z}_R = \frac{h(z,\varepsilon)}{1+\delta_\eta}\left[\left(\dot{x}-(1+\delta_v)\right)\left(\beta\lfloor\dot{x}\rfloor|z|^{n-1}+\gamma(\dot{x}|\dot{z}|)^n\right)\right] \quad (10)$$

where δ_η and δ_v respectively control the stiffness degradation and the strength degradation. The function $h(z,\varepsilon)$ managed the pinching effect is represented by

$$\begin{aligned} h(z,\varepsilon) &= 1-\xi_s(1 \\ &- e^{-p\varepsilon})exp\left[-\left(\frac{z\cdot sgn(x)-\frac{q}{[(1+\delta_v\varepsilon)(\beta+\gamma)]^{1/n}}}{x[\lambda+\xi_s(1-e^{-p\varepsilon})(\psi+\delta_{\psi\varepsilon})]}\right)^2\right] \end{aligned} \quad (11)$$

where ξ_s controls the extent of the total slip, q is the initial amount of pinching, p is the pinching slope, ψ is the parameter that contributes to the amount of pinching, δ_ψ is the parameter for the rate of the pinching spread, λ is the pinching ratio, ε is the hysteretic energy.

3.2 Extended Bouc-Wen model with self-centering effect

The hysteretic curves of the RC structure with SCEBs behave the flag-shaped behavior with energy dissipation ability and self-centering capability as mentioned in previous studies (Ozbulut and Hurlebaus 2012, Erochko *et al.* 2013). Because the structure with SCEB can be regarded as the SCEB system and the RC structure system assembled in parallel, as mentioned in Section 2. Based on the unique self-centering effect and degradation of the RC structure with SCEB, an extended Bouc-Wen model with the self-centering effect is established to predict the nonlinear response of such structure system. The extended model is expressed as

$$\begin{aligned} m\ddot{x}+c\dot{x}+a_Rk_{R1}x+(1-a_R)k_{R1}z_R+k_{s1}x_{sy}sgn(u) \\ +k_{s2}x+a_bk_{b1}x+(1-a_b)k_{b1}z_b \\ =F \end{aligned} \quad (12)$$

where a_R is the ratio of the post-yield stiffness (k_{R2}) and pre-yield stiffness (k_{R1}) of the RC structure, x_{sy} is the yield displacement of the self-centering system.

(1) Based on the Bouc-Wen model, the restoring force of the RC structure (F_R) is given by

$$F_R = a_Rk_{R1}x+(1-a_R)k_{R1}z_R \quad (13)$$

where $\dot{z}_R$ is an evolutionary variable to account for the hysteresis property considering the degradation and pinching effects, which can be expressed as

$$\begin{aligned} \dot{z}_R = \frac{h(z_R,\varepsilon_R)}{1+\delta_{R\eta}}[(\dot{x}-(1+\delta_{Rv}))(\beta_R\lfloor\dot{x}\rfloor|z_R|^{n_R-1}z_R \\ +\gamma_R(\dot{x}|\dot{z}_R|)^{n_R})] \end{aligned} \quad (14)$$

(2) The restoring force (F_s) offered by the self-centering group in the SCEB can be expressed as follows

$$F_s = \begin{cases} k_{s1}x & 0\le|x|<|x_{sy}| \\ k_{s1}x_{sy}sgn(x)+k_{s2}x & |x|\ge|x_{sy}| \end{cases} \quad (15)$$

$$k_{s1} = k_{out}k_{in}/(k_{out}+k_{in}) \quad (16)$$

$$x_{sy} = f_{sy}/k_{s1} \quad (17)$$

where k_{out} and k_{in} are the stiffness of the outer tube and inner tube of the SCEB system, respectively.

(3) According to the Bouc-Wen model, the restoring force of the BRB system (F_b) is calculated by

$$F_b = a_bk_{b1}x+(1-a_b)k_{b1}z_b \quad (18)$$

where a_b is the ratio of the post-yielding stiffness to the pre-yielding stiffness of the BRB system, $\dot{z}_b$ is an evolutionary variable to account for the hysteresis property without the degradation and pinching effects, which can be given by

$$\dot{z} = \dot{x}-\beta_b|\dot{x}\cdot z_b|{z_b}^{n_b-1}-\gamma_b\cdot\dot{x}\cdot{z_b}^{n_b} \quad (19)$$

Fig. 5 shows the elevation view of the steel core in the BRB. The elastic stiffness k_{b1} of the BRB considering the variation of cross sectional area along the length of the brace can be accurately predicted by

$$k_{b1} = \frac{EA_jA_yA_t}{A_jA_tL_y+2A_yA_tL_j+2A_yA_jL_t} \quad (20)$$

The post-yielding stiffness k_{b2} of the BRB is expressed as

$$k_{b2} = a_bk_{b1} \quad (21)$$

where a_b is the ratio of post-yield stiffness to pre-yield stiffness, a_b=0.02.

4. Extended model validation

4.1 Model implementation

To validate the feasibility of the extended Bouc-Wen model with self-centering effect, simulation analyses of the extended model under the sine wave excitations were

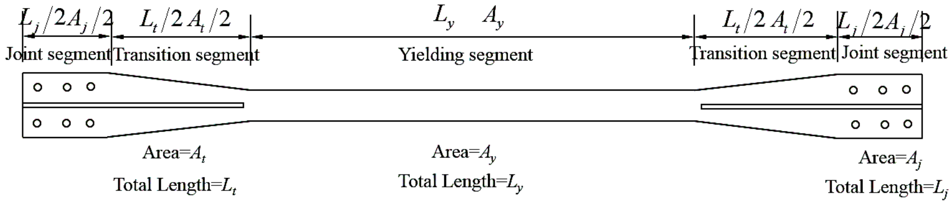

Fig. 5 Elevation view of the steel core in the BRB

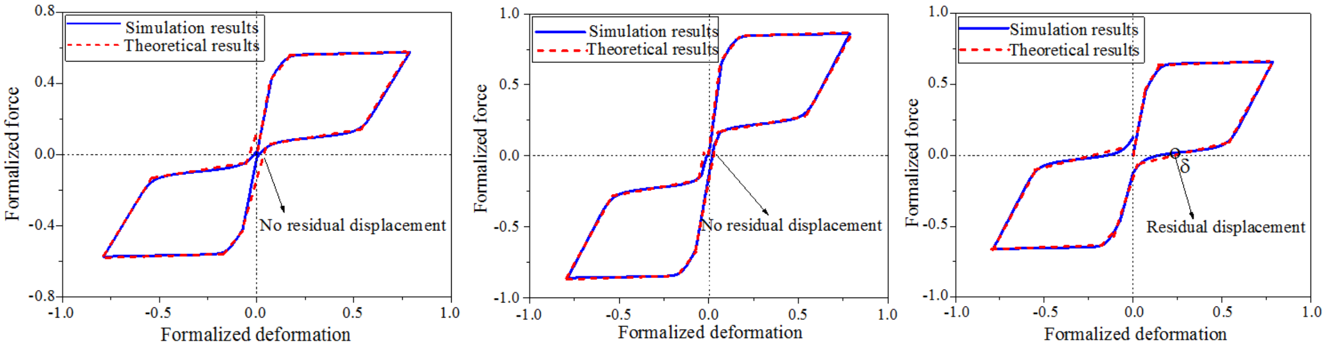

(a) (b) (c)

Fig. 6 Comparisons of hysteresis curves between the simulation results and the theoretical results

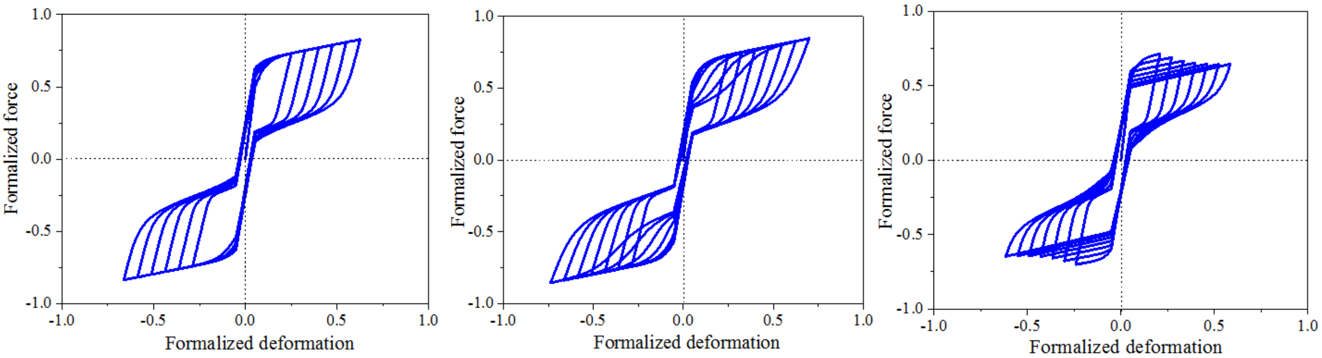

(a) without degradation (b) with stiffness degradation (c) with strength degradation

Fig. 7 Hysteresis curves based on the extended Bouc-Wen model

conducted by programming in the MATLAB/Simulink environment. Fig. 6 shows the hysteresis curves of the SCEB structure with different self-centering force based on the extended Bouc-Wen model and the corresponding theoretical hysteresis curves as mentioned in the previous study (Dong *et al.* 2017). It can be seen that the extended Bouc-Wen model is capable of capturing the excellent self-centering capability and the stable energy dissipation ability of the RC structure with SCEBs. As shown in Figs. 6(a) and (b), the residual deformation of the RC structure with SCEBs is very small neglected to zero when the self-centering force in SCEB is greater than or equal to the yielding force of the RC structure. In contrast, when the self-centering force in SCEB is less than the yielding force of the RC structure, the large residual displacement (δ) of the RC structure is observed, as shown in Fig. 6(c). The comparison results indicate that the extended model can accurately predict the hysteretic curves of the SCEB structure with different self-centering force.

The hysteretic curves based on the extended Bouc-Wen model without degradation are shown in Fig. 7(a). It can be seen that the stiffness degradation and strength degradation are not observed for the hysteretic curves. Fig. 7(b) presents the hysteretic curves based on the extended model considering the stiffness degradation. As shown, when only the stiffness degradation is considered, the stiffness of each hysteresis loop decreases with the increase of the cycle number. The hysteresis curves considering only strength degradation are shown in Fig. 7(c), the stiffness of each loop is the same, while the strength of each hysteresis loop decreases progressively. Overall, the extended model can successfully simulate the unique self-centering and degradation characteristics of the RC structure with SCEB.

4.2 Parameter identification

In order to verify the accuracy of the extended model, the parameter identification is requisite. In this study, UKF based on the unscented transform (UT) technique was used for the parameter identification of the extended Bouc-Wen model. A set of carefully chosen sample points called sigma points is used for the UKF to present the state vector (Chatzi and Smyth 2009). These sigma points can completely capture the posterior mean and covariance of

Gaussian random variable with the 3rd-order Taylor series expansion for any nonlinearity (Xiong *et al*. 2006, Xie and Feng 2012).

To implement the UKF method for the system identification problem, the discrete nonlinear difference state space equation is expressed as

$$X_{k+1} = F(X_k, u_k, w_k) \tag{22}$$

$$Y = H(X_k, v_k) \tag{23}$$

in which w_k is the discrete process noise assumed to be a Gaussian white noise with zero mean and a covariance matrix Q, and v_k is the measurement noise also assumed to be Gaussian white noise with zero mean and a covariance matrix R. Function F is as follows

$$F(X_k, u_k, w_k) = X_k + \int_{k\Delta t}^{(k+1)\Delta t} f(X(t), u(t), w(t))dt \tag{24}$$

And then the above integration can be evaluated by using numerical methods such as fourth-order Runge-Kutta method.

To implement the UKF algorithm, the state vector is redefined as the concatenation of the original state vector and noise variables as

$$X_k^a = [X_k^T, w_k^T, v_k^T]^T \tag{25}$$

Start with the initialization

$$\hat{X}_0 = E[X_0] \tag{26}$$

$$P_0 = E\left[(X_0 - \hat{X}_0)(X_0 - \hat{X}_0)^T\right] \tag{27}$$

$$\hat{X}_0^a = E[X^a] = \left[\hat{X}_0^T \; 0 \; 0\right]^T \tag{28}$$

$$P_0^a = E\left[(X_0 - \hat{X}_0)(X_0 - \hat{X}_0)^T\right] = \begin{bmatrix} P_0 & 0 & 0 \\ 0 & Q & 0 \\ 0 & 0 & R \end{bmatrix} \tag{29}$$

The augmented state vector for Equation (12) is expressed as

$$X = \left[z, \varepsilon, k, c, \alpha, \beta, \gamma, n, \delta_v, \delta_\eta\right]^T \qquad (24)$$

The systematic observation is the restoring force

$$Y = F \tag{31}$$

The state space equation is formulated based on (10) as follows

$$f(X(t), u(t)) = \begin{bmatrix} \dfrac{\dot{x} - (1+\delta_v)[\beta|\dot{x}||z|^{n-1} + \gamma\dot{x}|z|^n]}{1+\delta_\eta} \\ 0 \\ 0 \\ 0 \\ 0 \\ 0 \\ 0 \\ 0 \\ 0 \\ 0 \end{bmatrix}^T \tag{32}$$

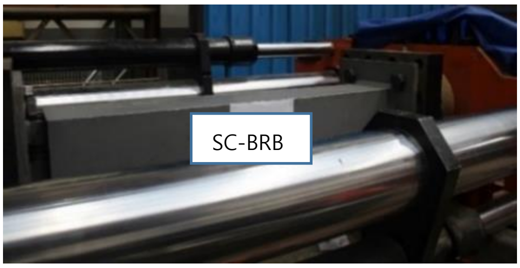

(a) test setups

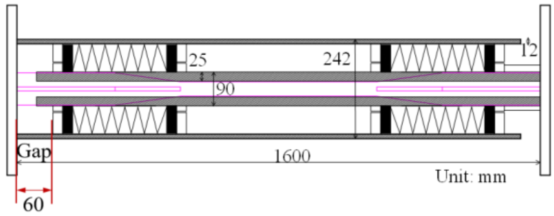

(b) dimensions

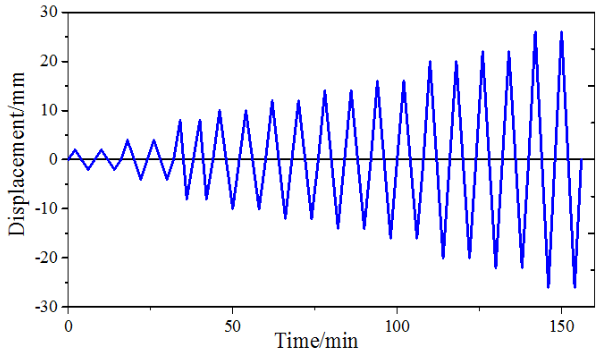

(c) Loading protocol

Fig. 8 SCEB

4.3 Experimental validation of the extended model without degradation

To validate the availability of the extended Bouc-Wen model without degradation, this extended model is validated by the experimental results of the SCEB. The SCEB was tested using the 3,000 kN servo hydraulic test system as shown in Fig. 8(a). For the SCEB system as mentioned in Section 2, the inner and outer tubes must be capable of bearing the axial force without failure or yielding for the system to function. Therefore, Q345 steel was selected for the inner and outer tubes due to its large compressive and yield strengths. The steel core was made of Q235 steel due to its great deformability for energy dissipation. The yielding strength, ultimate strength and ultimate strain of Q235 were obtained from tests and the values were 297 MPa, 421 MPa and 35.3%, respectively. Q345 steel was with a yielding strength of 435 MPa obtained from the material characteristic test. The length of the specimen was 1600 mm. 18 groups of disc springs with each group consisting of 4 pieces (totally 72 pieces) were installed to series in the tests. Fig. 8(b) shows the dimensions of the SCEB and Table 1 summarizes the primary design parameters. The test employed a displacement-control loading scheme with two cycles at each target displacement as shown in Fig. 8(c).

Table 1 Design parameters of the SCEB

Specimen	Specimen length (mm)	Steel core (mm)	Outer tube (mm)		Inner tube (mm)		End plate (mm)	Pre-compressive force (kN)
			Cross section	Wall thickness	Cross section	Wall thickness		
SCEB	1600	40×5	240×240	10	90×40	16	300×300×30	370

Table 2 Parameter values of the extended model for the SCEB

Specimen	k_{b1} (kN/mm)	α_b	β_b	γ_b	n_b	u_{sy} (mm)	k_{s1} (kN/mm)	k_{s2} (kN/mm)
SCEB	36	0.02	0.5	0.5	2.0	5.0	84.1	11.5

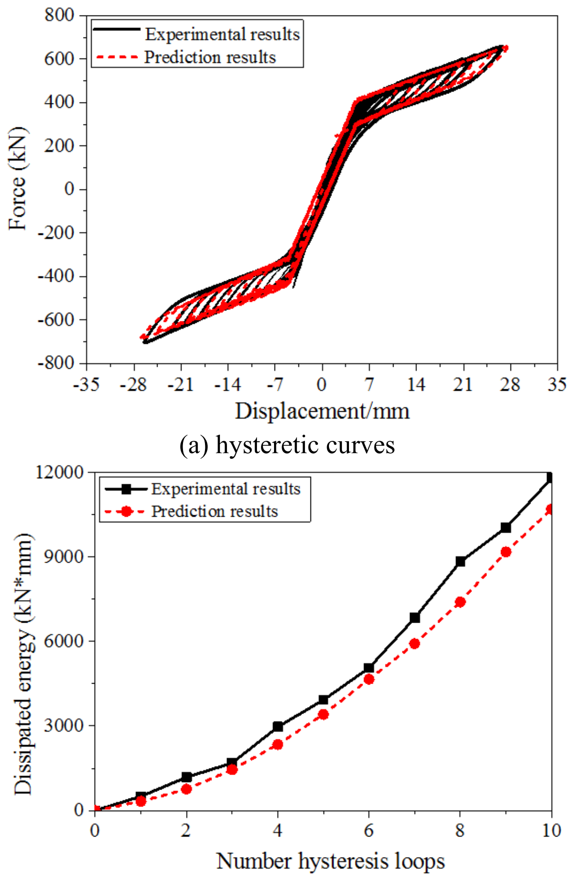

(a) hysteretic curves

(b) dissipated energy

Fig. 9 Comparisons of the experimental and predicted results of the SCEB

For finding a quantitative comparison basis between the prediction results and experimental results, the relative error is used in this study. The relative error is set as

$$J_{re} = \frac{|A_e - A_p|}{|A_e|} \times 100\% \tag{33}$$

where A_e and A_p are the values of the experimental results and the prediction results, respectively.

Table 2 lists the corresponding parameter values of the extended model for the SCEB, and they are defined based on the design parameters of the SCEB and the parameter identification using UKF as mentioned in Section 4.2. Fig. 9 shows the comparisons of the hysteresis curves of the SCEB between experimental results and prediction results based on the extended Bouc-Wen model, which are represented by solid lines and dotted lines, respectively. To quantitatively examine the results, these results and the corresponding errors with respect to the testing data are summarized in Table 3.

Table 3 Relative error associated with the comparison between prediction results and experiment results of the SCEB

Specimen		f_{max} (kN)	J_{re} (%)	f_{SCEBy} (kN)	J_{re} (%)	δ (mm)	J_{re} (%)	u_{SCEBy} (mm)	J_{re} (%)	k_{SCEB2} (kN/mm)	J_{re} (%)
SCEB	Experiment	685.2	3.6	420.5	2.3	0.9	11.1	5.0	6.0	11.5	6.9
	Prediction	660.8		410.7		0.8		4.7		10.7	

where A_e and A_p are the values of the experimental results and the prediction results, respectively.

Table 2 lists the corresponding parameter values of the extended model for the SCEB, and they are defined based on the design parameters of the SCEB and the parameter identification using UKF as mentioned in Section 4.2. Fig. 9 shows the comparisons of the hysteresis curves of the SCEB between experimental results and prediction results based on the extended Bouc-Wen model, which are represented by solid lines and dotted lines, respectively. To quantitatively examine the results, these results and the corresponding errors with respect to the testing data are summarized in Table 3.

Fig. 9(a) shows the displacement-force hysteretic curves of the SCEB system. As shown, the SCEB system exhibits the typical flag-shaped hysteretic behavior with the excellent self-centering capability and the stable energy dissipation ability, and the hysteretic curves in positive and negative displacement directions are symmetrical. The very small residual deformation (0.9 mm) is observed for the SCEB. It should be noted that the hysteretic curves of the SCEB are without obvious strength and stiffness degradations. The predicted curves as shown in Fig. 9(a) agree well with experimental results, especially the self-centering effect. The relative errors of the parameter values between numerical and experimental results are below 11.1%, as shown in Table 3. Hence, the comparison results show that force-displacement relationship curves of the SCEB derived from the extended model agree well with experimental results. It can be seen from Fig. 9(b), the errors of energy dissipated between prediction and experiment do not exceed 10%. Overall, the extended model is able to predict the experimental force-displacement response of the SCEB with good precision.

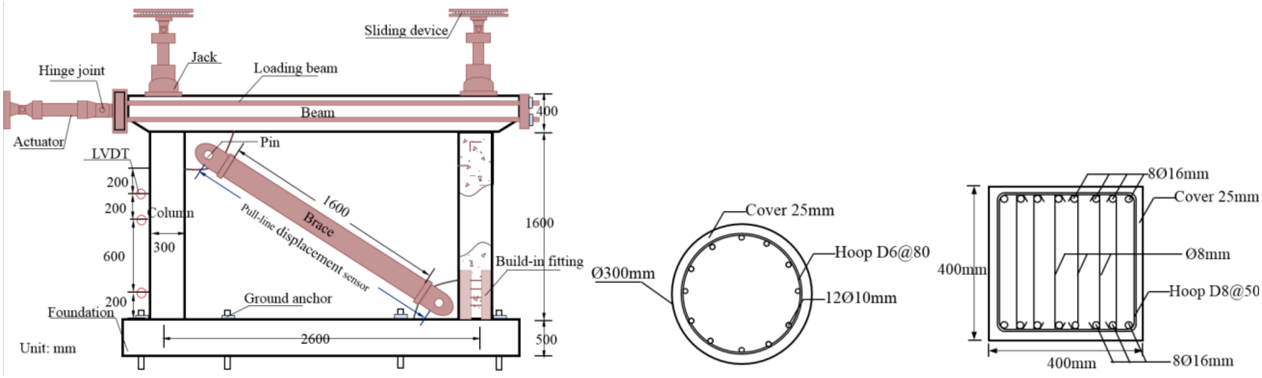

(a) general view (b) A-A section of the column (c) B-B section of the cap beam

Fig. 10 Details of the RC structure specimen

Table 4 Design parameters of the two specimens

Specimen	Brace	Span (mm)	Column height (mm)	Axial load ratio	Longitudinal reinforcement		Transverse reinforcement		
					Dimeter (mm)	Reinforcement ratio	Dimeter (mm)	Spacing (mm)	Transverse reinforcement ratio
RC frame	-	2600	1600	0.15	10	1.3%	6	100	0.6%
RC frame with SCEB	SCEB	2600	1600	0.15	10	1.3%	6	100	0.6%

4.4 Experimental validation of the extended model with degradation

To validate the accuracy of the extended model with degradation, the model is validated by the experimental results of the RC structure with SCEB. Large-scale experiments of the RC frames without and with SCEB were carried out at the Key Laboratory of Urban Security and Disaster Engineering of Ministry of Education in Beijing University of Technology. Fig. 10(a) shows a general view of the scaled specimen. As shown, the diameter of each circular column is 300 mm and the height is 1600 mm. The center-to-center distance between the two columns is 2600 mm. The cross-section of the square beam is 400 mm×400 mm and the length is 3600 mm. C40 concrete was used for the specimen. The compressive strength of the concrete at 28 days was tested and the value was 35.3 MPa. Twelve rebars with a diameter of 10 mm are installed along the column, and the longitudinal reinforcement ratio is 1.3%. The diameter of the stirrup is 6 mm and the space between adjacent stirrups is 80 mm, which results in a transverse reinforcement ratio of 0.6%. The column has a 25 mm concrete cover over the reinforcement bars. Figs. 10(b) and (c) show the cross sections of the column and the beam, respectively. Table 4 lists the design parameters of the two specimens, including the axial load ratio, longitudinal reinforcement ratio and transverse reinforcement ratio.

The photo of the test setup and the specimen is illustrated in Fig. 11(a). As shown, one actuator is horizontally installed to provide the cyclic load to the specimen and two hydraulic jacks are used to provide the vertical load. In the present study, the vertical load provided by the two jacks is 15% of the axial load carrying capacity of the column, i.e. $0.15f_c'A_g$ (Imbsen 2007), in which f_c' is the concrete compressive strength, and A_g is the cross section area of the columns. The vertical load provided by each jack is therefore 202.4 kN based on the information provided in Fig. 10(a) and Table 4. The behaviors of the frame specimens with and without SCEB under the cyclic loadings were tested. The loading protocol as suggested by the Chinese Specification of Testing Methods for Earthquake Resistant Structures is shown in Fig. 11(b). It should be noted that the frame without SCEB was applied with a displacement of around 90 mm, while only a displacement of 52 mm is applied for the specimen with SCEB. This is because the displacement capacity of the frame with SCEB is affected by the deformability of the SCEB, and the displacement capacity of the SCEB is controlled by the gap between the end plate and the plate at the end of the disc spring as shown in the Fig. 8(b). The gap of the SCEB was not very well designed in the tests, and it was only 60 mm, which constrained the deformation capability of the brace. When the brace with larger allowable displacement is designed, the same or even better displacement capacity can be achieved.

Table 5 lists the corresponding parameter values of the extended model with stiffness and strength degradation based on the design parameters of the structures and the parameter identification using UKF as mentioned in Section 4.2. Moreover, the model parameters of the SCEB remain unchanged as mentioned in Section 4.3. The recorded lateral load-deformation hysteretic curves of the RC frame are presented in Fig. 12(a). As shown, the hysteretic curves of the RC structure without SCEB are plump and with obvious stiffness and strength degradations due to the severe concrete and rebar damages at the top and bottom of the columns. This result coincides well with many previous studies (e.g. (Bazaez and Dusicka 2016)). The hysteretic curves also show that the large residual displacement existed in the RC frame after the test. As shown in Fig. 12(a), when a displacement of 88 mm is applied to the

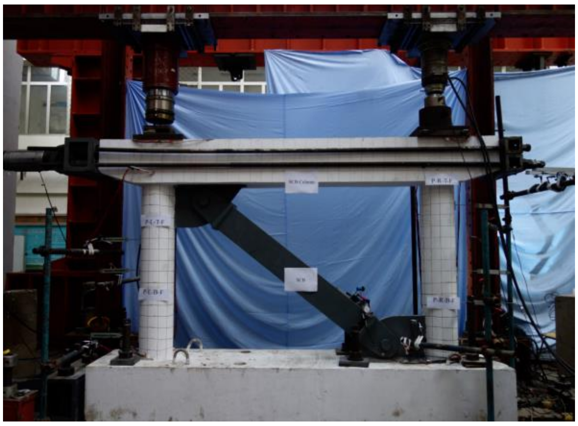

(a)

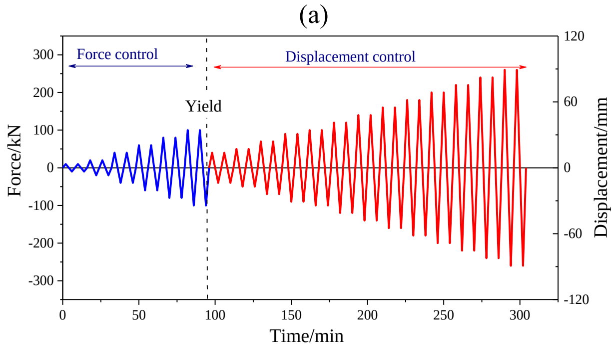

(b)

Fig. 11 Comparisons of the experimental and predicted results of the SCEB

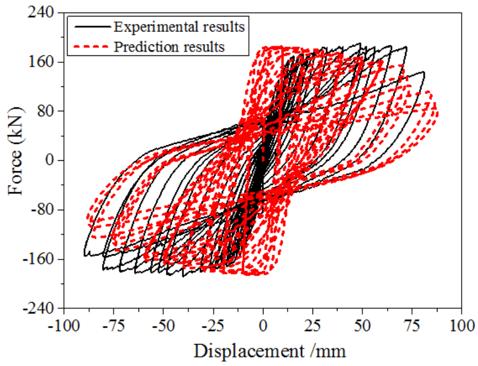

(a) hysteretic curves

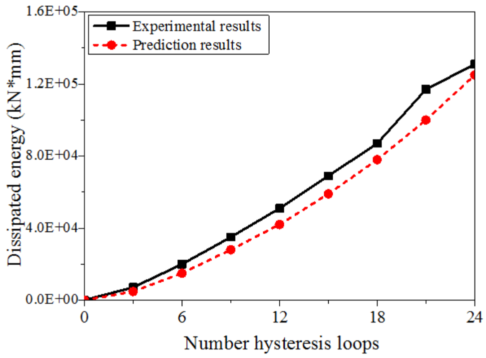

(b) dissipated energy

Fig. 12 Comparisons between the experimental and predicted results of RC frame

Table 5 Parameter values of the extended models for the RC frame and the RC frame with SCEB

Specimen	α_R	β_R	γ_R	n_b	δ_η	δ_υ	q	p	ψ	δ_ψ	λ	k_{R1} (kN/mm)
RC frame/ RC frame with SCEB	0.05	0.4	-0.6	2.0	0.05	0.1	0.15	2.5	0.3	0.001	0.25	10.8

specimen, the residual displacements in the negative and positive displacement directions are -72 mm and 69 mm, respectively.

The lateral load-deformation hysteretic curves of the structure with SCEB are shown in Fig. 13(a). It can be seen that the structure with SCEB exhibited a flag-shaped hysteretic curve with excellent self-centering capability. This figure also shows that the SCEB system can effectively increase the strength and the stiffness of the RC structure. The residual displacements are only 7.6 mm and 8.4 mm in the positive and negative directions respectively when the ultimate displacement of 52 mm is applied. It should be noted that the hysteresis behavior of the frames with SCEB behaves no great strength degradation as shown in Fig. 13. However, the slight strength degradation can be observed. This is because that the hysteresis curves of the frame with SCEB is the summation of that of the frame and that of the SCEB, and the RC frame behaves obvious strength degradation and the SCEB has no significant degradation.

Figs. 12(a) and 13(a) show the comparisons of the hysteretic curves of the RC structure without and with SCEB between the predicted results and the experimental results. The black full lines represent the experimental results and the red dot lines stand for the predicted results. It can be seen that in general good matches are obtained, which demonstrates the accuracy of the extended model. As shown, the initial stiffness, the post-yielding stiffness, the yield displacement and the corresponding force of the tested specimens are well captured by the predicted results. In particular, the extended model is capable of capturing the structural self-centering and energy dissipation capabilities of the structure with SCEB.

To quantitatively examine the results, the predicted results and the corresponding errors with respect to the testing data are summarized in Table 6. For experimental results, the peak forces of the structure with SCEB in the positive and negative directions are 983 kN and 1037 kN, respectively. In comparison, the peak forces of the predicted model in the positive and negative directions are 967 kN and 945 kN, respectively. The errors of the peak forces between the experimental results and the predicted results in the positive and negative directions are only 1.6% and 8.8%, respectively. The errors of the dissipated energy for the structures without and with SCEB are also quite small as shown in Figs. 12(b) and 13(b). For the residual displacements (δ), the errors of the experimental and predicted results for the structure without SCEB are very small (the errors in the positive displacement direction and negative displacement direction are only 9.2% and 10.2%, respectively). However, for the structure with SCEB, the errors in the positive and negative displacement directions are slightly large. This is because the absolute experimental

Table 6 Relative error associated with the comparison between prediction results and experiment results of the RC frame and the RC frame with SCEB

Specimen		F_{max} (kN)		J_{re} (%)		F_y (kN)		J_{re} (%)		δ (mm)		J_{re} (%)	
RC frame	Experiment	-193	188	5.8	8.4	141	136	13.4	16.2	-65	64	9.2	10.9
	Prediction	-178	193			160	158			-59	71		
RC frame with SCEB	Experiment	-1037	983	8.8	1.6	-460	480	8.9	5.8	-8.6	7.4	16.3	31.1
	Prediction	-945	967			501	452			-7.2	5.1		

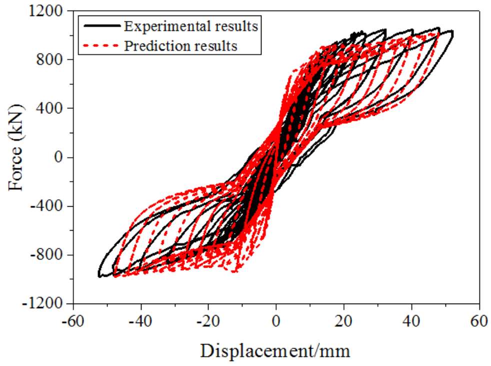

(a) hysteretic curves

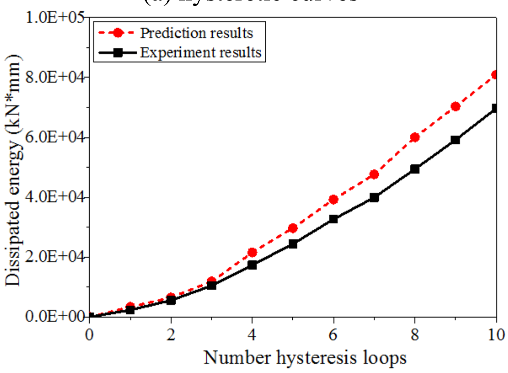

(b) dissipated energy

Fig. 13 Comparisons of the experimental and predicted results of the RC frame with the SCEB

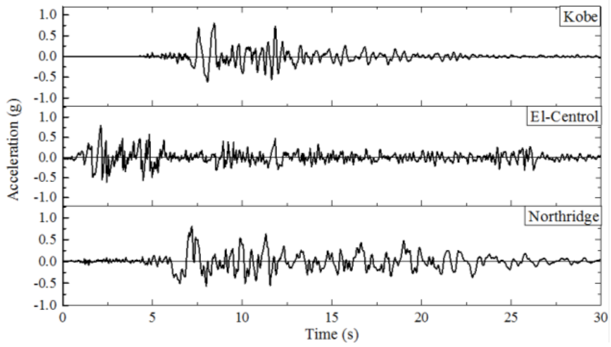

Fig. 14 Ground acceleration time histories

values are quite small, which are 7.4 mm and 8.6 mm respectively in the positive and negative displacement directions. Very small variation of the absolute value can lead to obvious large differences in percentage. Overall, the extended model is able to predict the experimental force-displacement response of the structure with SCEB with good precision. These comparisons verify the reliability of the extended model in simulating the nonlinear responses of the RC structure with SCEB.

5. Extended model application in nonlinear time history analysis

The above numerical results present that the extended Bouc-Wen model can well simulate the hysteresis characteristics of the RC structure with SCEB. Further investigation is required to understand the seismic responses of the RC structure with SCEB under seismic loadings. For comparison, the seismic responses of the RC structure without SCEB are also calculated and discussed.

The prototype RC frame is selected as an example for the analysis. The height of each column is 4.8 m, and the diameter of the circular column is 0.9 m. The center-to-center distance between two columns is 7.8 m. In the column, 18 longitudinal rebars with a diameter of 24 mm are installed evenly in the cross section. The diameter of the stirrups is 10 mm and the spacing between adjacent stirrup is 65 mm. These rebars result in a longitudinal reinforcement ratio of 1.3% and a transverse reinforcement ratio of 0.6%. The addition of the brace to the structure influences the dynamic characteristics of the frame in the transverse direction, so only the seismic excitation in the transverse direction is considered in the numerical simulation (Dong *et al.* 2017). Considering the requirements of the relevant Chinese seismic design code, three actual acceleration records were selected: Kobe earthquake record, El-Centro earthquake record and Northridge earthquake record. Fig. 14 shows the acceleration time histories of the ground motions. To more clearly understand the influence of the SCEB on the structural seismic performance, the PGA of these three ground motions is scaled to 0.8 g in the numerical simulation.

Fig. 15 shows the seismic responses of the RC structures without and with SCEB under three earthquake motions, and the corresponding peak values are summarized in Table 7. Fig. 16 presents the hysteretic curves of the RC frame and the RC frame with SCEB subjected to the three earthquake records. It should be noted that the duration of the three earthquake loadings shown in Fig. 14 is 30 s. To capture the residual displacement, the simulations are carried out until the RC structure becomes stable. As shown in Fig. 15, the RC structure almost stops vibrating when the time reaches 40 s under these three earthquake loadings. Fig. 15 also shows that the extended Bouc-Wen model with self-centering effect is robust for seismic responses

Table 7 Seismic responses of the RC frames without and with SCEB under earthquake actions

Conditions	Residual displacement (mm)			Peak displacement (mm)			Peak acceleration (g)		
	Kobe	EL-Contro	Northridge	Kobe	EL-Contro	Northridge	Kobe	EL-Contro	Northridge
RC frame	23.1	3.9	21.5	208	129	149	1.46	0.91	1.38
RC frame with SCEB	3.0	0.5	0.7	76	94	102	1.58	0.99	1.59

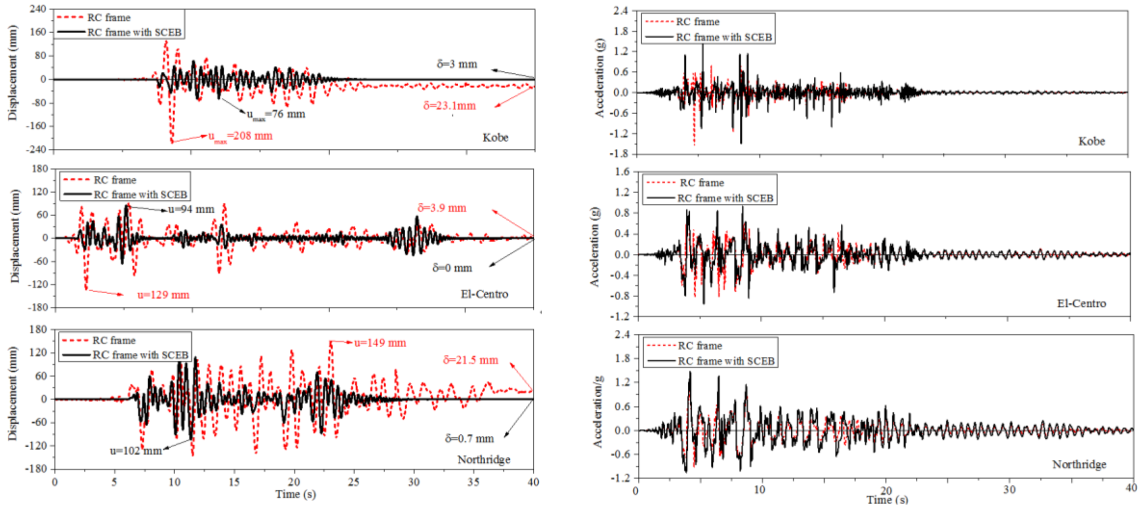

(a) displacement (b) acceleration

Fig. 15 Seismic responses of RC frame and RC frame with SCEB subjected to the three earthquake records

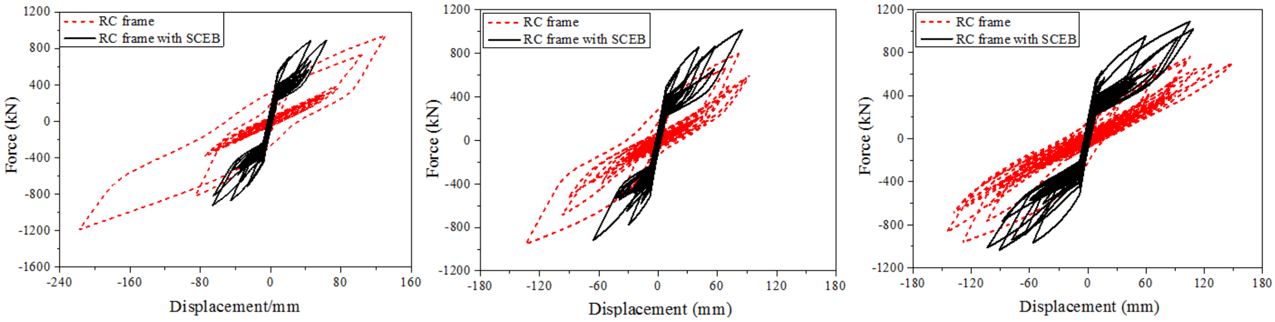

(a) Kobe earthquake (b) El-Centro earthquake (c) Northridge earthquake

Fig. 16 Hysteretic curves of RC frame and RC frame with SCEB subjected to three earthquake records

prediction in dynamic analysis of the RC structure with SCEB.

Fig. 15(a) shows the displacement time histories of the RC structures without and with SCEB under seismic loadings. As expected, when the SCEB is used to the RC structure, much smaller residual displacements are obtained as compared with the RC structure without SCEB. As shown, the residual displacements of the RC structure without SCEB are 23.1 mm, 3.9 mm and 21.5 mm respectively under the three earthquake grounds. When the SCEB is used, the corresponding values reduce to 3.0 mm, 0.5 mm and 0.7 mm, with the reduction ratio reaching 87.0%, 87.2% and 96.7% respectively. This is due to the excellent self-centering capability of the SCEB, which behaves a typical flag-shaped hysteresis behavior, as shown in Fig. 16.

It can be seen from Fig. 15(a) and Table 7, the influence of the SCEB on the peak displacement responses of the RC structures is also very obvious. The SCEB can effectively decrease the peak displacement responses of the RC structure. For the RC structure with SCEB, the reduction ratio of the peak displacement are 63.5%, 27.1% and 31.5% respectively with an average of 40.7% for the three earthquake ground motions. This better performance is mainly attributed to higher elastic lateral stiffness and better energy dissipation capability of the SCEB.

The acceleration time histories of the RC structure without and with SCEB are shown in Fig. 15(b), the corresponding peak values are tabulated in Table 7. It can be seen that the acceleration of the RC structure with SCEB is slightly larger than that of the RC structure without SCEB. As shown, the peak accelerations are 1.46 g, 0.91 g and 1.38 g respectively for the RC structure without SCEB. When the SCEB is used, the corresponding values increase to 1.58 g, 0.99 g and 1.59 g, with the rate of increase only reaching 8.2%, 8.8% and 15.2% respectively. The results are consistent with several previous studies, for example, the previous study by Christopoulos (2008) present that the self-centering energy dissipative brace tends to increase the peak acceleration response of the structure due to the large stiffness and the sharp transitions between the elastic and inelastic response. Fig. 16 shows the hysteretic curves of the RC structures without and with SCEB subjected to three earthquake records. It is apparent that the SCEB can amplify the stiffness of the RC frame, and the hysteresis behaviors of the structures with SCEB behave sharper transitions between the elastic and inelastic response. Fig. 16 also shows that the RC structure with SCEB behaves the excellent self-centering ability and the stable energy dissipation capability for the nonlinear dynamic analyses.

6. Conclusions

The SCEB with the excellent self-centering ability can be utilized in RC structures to minimize the residual deformation of the structure. To effectively predict the seismic responses of the RC structures with SCEBs, a mathematical method based on Bouc-Wen model was developed. The extended model is simple and effective, especially can be used to simulate the dynamic responses of the RC structure with SCEB. The extended Bouc-Wen model is capable of capturing the self-centering effect and the degradations of the RC structure with SCEB by programming in the Matlab/Simulink environment. Furthermore, the extended model can accurately predict the force-displacement hysteretic behavior of the RC structure using SCEB with different self-centering forces.

To validate the availability of the extended Bouc-Wen model, large-scale experimental studies of the SCEB and the RC structure without and with SCEB were carried out. The predicted results using the UKF for the parameter identification were compared with the experimental results. The comparison results reveal the hysteretic behavior obtained from the extended model could be good agreement with the experimental results. The extended Bouc-Wen model was viewed to be reasonably accurate as the force and the residual displacement values of the RC structure with SCEB. Furthermore, a series of nonlinear time history analyses based on the extended Bouc-Wen model were performed to investigate the effect of the SCEB on the seismic performance of the RC structure. Numerical results demonstrated that the RC structure equipped with SCEB showed much smaller residual displacement compared to the RC structure without SCEB. Numerical results also indicated that the SCEB system tended to amplify the peak acceleration of the RC structure. Given the analysis results obtained in this article, the extended Bouc-Wen model with self-centering effect is robust. Moreover, the extended model is capable of accurately predicting the hysteretic behavior of the RC structure with SCEB with strength and stiffness degradations and self-centering effect.

Acknowledgements

The authors acknowledge the partial support from the National Key Research Program of China (No. 2017YFE0103000), Beijing Municipal Education Commission (No. IDHT 20190504) and the National Science Foundation of China (No. 51421005, No. 51578022 and No. 51778023).

References

Ajrab, J.J., Pekcan, G. and Mander, J.B. (2004), “Rocking wall–Frame structures with supplemental tendon systems”, *Journal of Structural Engineering*, **130**(6), 895-903.

Araki, Y., Shrestha, K.C., Maekawa, N., Koetaka, Y., Omori, T. and Kainuma, R. (2016), “Shaking table tests of steel frame with superelastic Cu–Al–Mn SMA tension braces”, *Earthq. Eng. Struct. Dynam.*, **45**(2), 297-314. https://doi.org/10.1002/eqe.2659.

Baber, T.T. and Noori, M.N. (1985), “Random vibration of degrading, pinching systems”, *J. Eng. Mech.*, **111**(8), 1010-1026. https://doi.org/10.1061/(ASCE)0733-9399(1985)111:8(1010).

Baber, T.T. and Wen, Y.K. (1981), “Random vibration hysteretic, degrading systems”, *J. Eng. Mech. Divison*, **107**(6), 1069-1087.

Bazaez, R. and Dusicka, P. (2016), “Cyclic behavior of reinforced concrete bridge bent retrofitted with buckling restrained braces”, *Eng. Struct.*, **119**, 34-48. https://doi.org/10.1016/j.engstruct.2016.04.010.

Bouc, R. (1967), “Forced vibrations of mechanical systems with hysteresis”, *Proceedings of the Fourth Conference on Nonlinear Oscillations*, Prague, Czechoslovakia.

Carboni, B., Lacarbonara, W. and Auricchio, F. (2014), “Hysteresis of multiconfiguration assemblies of nitinol and steel strands: experiments and phenomenological identification”, *J. Eng. Mech.*, **141**(3). https://doi.org/10.1061/(ASCE)EM.1943-7889.0000852.

Chang, C., Strano, S. and Terzo, M. (2016), “Modelling of hysteresis in vibration control systems by means of the Bouc-Wen model”, *Shock Vib.*, 2016. http://dx.doi.org/10.1155/2016/3424191.

Chatzi, E.N. and Smyth, A.W. (2009), “The unscented Kalman filter and particle filter methods for nonlinear structural system identification with non-collocated heterogeneous sensing”, *Struct. Control Health Monitor.*, **16**(1), 99-123. https://doi.org/10.1002/stc.290.

Chou, C.C. and Chen, Y.C. (2012), “Development and seismic performance of steel dual-core self-centering braces”, *Proceedings of 15th World Conference on Earthquake Engineering*, Lisbon, Portugal, September.

Chou, C.C. and Chung, P.T. (2014), “Development and seismic tests of a cross-anchored dual-core self-centering brace using steel tendons as tensioning elements”, *Proceedings of the 10th National Conference on Earthquake Engineering*, Anchorage, Alaska, United States, July.

Chou, C.C. and Lai, Y.J. (2009), “Post-tensioned self-centering moment connections with beam bottom flange energy dissipators”, *J. Contruct. Steel Res.*, **65**(10), 1931-1941. https://doi.org/10.1016/j.jcsr.2009.06.002.

Christopoulos, C., Filiatrault, A., Uang, C. and Folz, B. (2002), “Posttensioned energy dissipating connections for moment-resisting steel frames”, *J. Struct. Eng.*, **128**(9), 1111-1120. https://doi.org/10.1061/(ASCE)0733-9445(2002)128:9(1111).

Christopoulos, C., Tremblay, R., Kim, H.J. and Lacerte, M. (2008), “Self-centering energy dissipative bracing system for the seismic resistance of structures: development and validation”, *J. Struct. Eng.*, **134**(1), 96-107. https://doi.org/10.1061/(ASCE)0733-9445(2008)134:1(96).

Clough, R. W., Benuska, K. L., and Wilson, E.L. (1965). “Inelastic earthquake response of tall buildings”, *Proceedings, Third World Conference on Earthquake Engineering*, New Zealand, January.

Dolce, M., Cardone, D. and Marnetto, R. (2000), "Implementation and testing of passive control devices based on shape memory alloys", *Earthq. Eng. Struct. Dynam.*, **29**(7), 945-968. https://doi.org/10.1002/1096-9845(200007)29:7%3C945::AID-EQE958%3E3.0.CO;2-%23.

Domaneschi, M. (2012), "Simulation of controlled hysteresis by the semi-active Bouc-Wen model", *Comput. Struct.*, **106**, 245-257. https://doi.org/10.1016/j.compstruc.2012.05.008.

Dong, H., Du, X., Han, Q., Hao, H., Bi, K. and Wang, X. (2017), "Performance of an innovative self-centering buckling restrained brace for mitigating seismic responses of bridge structures with double-column piers", *Eng. Struct.*, **148**, 47-62. https://doi.org/10.1016/j.engstruct.2017.06.011.

Dong, H. H., Du, X. L., Han, Q., Bi, K. M., Hao, H., (2019). "Hysteretic performance of RC double-column bridge piers with self-centering buckling-restrained braces", *Bullet. Earthq. Eng.*, https://doi.org/10.1007/s10518-019-00586-4.

Eatherton, M.R., Fahnestock, L.A. and Miller, D.J. (2014), "Computational study of self-centering buckling-restrained braced frame seismic performance", *Earthq. Eng. Struct. Dynam.*, **43**(13), 1897-1914. https://doi.org/10.1002/eqe.2428.

Eatherton, M.R., Ma, X., Krawinkler, H., Deierlein, G.G. and Hajjar, J.F. (2014), "Quasi-static cyclic behavior of controlled rocking steel frames", *J. Struct. Eng.*, **140**(11). https://doi.org/10.1061/(ASCE)ST.1943-541X.0001005.

Elbahey, S. and Bruneau, M. (2012), "Bridge Piers with Structural Fuses and Bi-Steel Columns. I: Experimental Testing", *J. Bridge Eng.*, **17**(1), 25-35. https://doi.org/10.1061/(ASCE)BE.1943-5592.0000234.

Erochko, J., Christopoulos, C. and Tremblay, R. (2014), "Design and Testing of an Enhanced-Elongation Telescoping Self-Centering Energy-Dissipative Brace", *J. Struct. Eng.*, **141**(6), https://doi.org/10.1061/(ASCE)ST.1943-541X.0001109.

Erochko, J., Christopoulos, C., Tremblay, R. and Choi, H. (2010), "Residual drift response of SMRFs and BRB frames in steel buildings designed according to ASCE 7-05", *J. Struct. Eng.*, **137**(5), 589-599. https://doi.org/10.1061/(ASCE)ST.1943-541X.0000296.

Erochko, J., Christopoulos, C., Tremblay, R. and Kim, H.J. (2013), "Shake table testing and numerical simulation of a self-centering energy dissipative braced frame", *Earthq. Eng. Struct. Dynam.*, **42**(11), 1617-1635. https://doi.org/10.1002/eqe.2290.

Foliente, G.C. (1995), "Hysteresis modeling of wood joints and structural systems", *J. Struct. Eng.*, **121**(6), 1013-1022. https://doi.org/10.1061/(ASCE)0733-9445(1995)121:6(1013).

Han, Q, Jia, Z.L., Xu, K., Zhou, Y.L., Du, X.L. (2019). "Hysteretic behavior investigation of self-centering double-column rocking piers for seismic resilience", *Eng. Struct.*, **188**, 218-232. https://doi.org/10.1016/j.engstruct.2019.03.024.

Huang, Y.C. and Tsai, K.C. (2002), "Experimental responses of large scale buckling restrained brace frames", CEER/R91-03; Center for Earthquake Engineering Research, National Taiwan Univ., Taiwan.

Imbsen, R. A. (2007), *AASHTO Guide Specifications for LRFD Seismic Bridge Design*", American Association of State Highway and Transport Officials, Subcommittee for Seismic Effects on Bridges, USA.

Kim, H.J. and Christopoulos, C. (2009), "Numerical models and ductile ultimate deformation response of post-tensioned self-centering moment connections", *Earthq. Eng. Struct. Dynam.*, **38**(1), 1-21. https://doi.org/10.1002/eqe.836.

Kitayama, S. and Constantinou, M.C. (2016), "Design and Analysis of Buildings with Fluidic Self-Centering Systems", *J. Struct. Eng.*, **142**(11), https://doi.org/10.1061/(ASCE)ST.1943-541X.0001583.

Kitayama, S. and Constantinou, M.C. (2017), "Fluidic Self-Centering Devices as Elements of Seismically Resistant Structures: Description, Testing, Modeling, and Model Validation", *J. Struct. Eng.*, **143**(7). https://doi.org/10.1061/(ASCE)ST.1943-541X.0001787.

Li, H., Mao, C.X. and Ou, J.P. (2008), "Experimental and theoretical study on two types of shape memory alloy devices", *Earthq. Eng. Struct. Dynam.*, **37**(3), 407-426. https://doi.org/10.1002/eqe.761.

Ma, H.W. and Cho, C.D. (2008), "Feasibility study on a superelastic SMA damper with re-centring capability", *Mater. Sci. Eng. A*, **473**(1), 290-296. https://doi.org/10.1016/j.msea.2007.04.073.

Ma, H.W. and Yam, M.C. (2011), "Modelling of a self-centring damper and its application in structural control", *J. Contruct. Steel Res.*, **67**(4), 656-666. https://doi.org/10.1016/j.jcsr.2010.11.014.

Ma, X., Eatherton, M., Hajjar, J., Krawinkler, H. and Deierlein, G. (2010) "Seismic design and behavior of steel frames with controlled rocking—Part II: Large scale shake table testing and system collapse analysis", *Proceedings of the 2010 Structures Congress*, Orlando, Florida, United States, May. https://doi.org/10.1061/41130(369)139.

McCormick, J., Aburano, H., Ikenaga, M. and Nakashima, M. (2008) "Permissible residual deformation levels for building structures considering both safety and human elements", *Proceedings of the 14th World Conference on Earthquake Engineering*, Beijing, China, October.

Miller, D.J., Fahnestock, L.A. and Eatherton, M.R. (2011), "Self-centering buckling-restrained braces for advanced seismic performance", *Proceedings of the 2011 Structures Congress*, Las Vegas, Nevada, April. https://doi.org/10.1061/41171(401)85.

Miller, D.J., Fahnestock, L.A. and Eatherton, M.R. (2012), "Development and experimental validation of a nickel-titanium shape memory alloy self-centering buckling-restrained brace", *Eng. Struct.*, **40**, 288-298. https://doi.org/10.1016/j.engstruct.2012.02.037.

Nicknam, A. and Filiatrault, A. (2015), "Direct Displacement-Based Seismic Design of Propped Rocking Walls", *Earthq. Spectra*, **31**(1), 179-196. https://doi.org/10.1193/051512EQS187M.

Ozbulut, O.E. and Hurlebaus, S. (2012), "Application of an SMA-based hybrid control device to 20-story nonlinear benchmark building", *Earthq. Eng. Struct. Dynam.*, **41**(13), 1831-1843. https://onlinelibrary.wiley.com/action/doSearch?ContribAuthorStored=Hurlebaus%2C+Stefan.

Ozbulut, O.E., Hurlebaus, S. and DesRoches, R. (2011), "Seismic response control using shape memory alloys: a review", *J. Intelligent Mater. Syst. Struct.*, **22**(14), 1531-1549.

Ricles, J.M., Sause, R., Peng, S. W. and Lu, L.W. (2002), "Experimental evaluation of earthquake resistant posttensioned steel connections", *J. Struct. Eng.*, **128**(7), 850-859. https://doi.org/10.1061/(ASCE)0733-9445(2002)128:7(850).

Saiidi, M. and Sozen, M.A. (1981), "Simple nonlinear seismic analysis of R/C structures", *J. Struct. Divison*, **107**(5), 937-953.

Sireteanu, T., Giuclea, M. and Mitu, A.M. (2010), "Identification of an extended Bouc-Wen model with application to seismic protection through hysteretic devices", *Comput. Mech.*, **45**(5), 431-441. https://doi.org/10.1007/s00466-009-0451-y.

Sivaselvan, M.V. and Reinhorn, A.M. (2000), "Hysteretic models for deteriorating inelastic structures", *J. Eng. Mech.*, **126**(6), 633-640. https://doi.org/10.1061/(ASCE)0733-9399(2000)126:6(633).

Takeda, T., Sozen, M.A. and Nielsen, N.N. (1970), "Reinforced concrete response to simulated earthquakes", *J. Struct. Divison*, **96**(12), 2557-2573.

Tremblay, R. and Christopoulos, C. (2012) "Self-centering energy dissipative brace apparatus with tensioning elements", US Patent 8,250,818,2012.

Tremblay, R., Lacerte, M. and Christopoulos, C. (2008), "Seismic response of multistory buildings with self-centering energy dissipative steel braces", *J. Struct. Eng.*, **134**(1), 108-120. https://doi.org/10.1061/(ASCE)0733-9445(2008)134:1(108).
Wen, Y. K. (1976), "Method for random vibration of hysteretic systems", *J. Eng. Mech. Divison*, **102**(2), 249-263.
Xie, Z.B. and Feng, J.C. (2012), "Real-time nonlinear structural system identification via iterated unscented Kalman filter", *Mech. Syst. Signal Process*, **28**, 309-322. https://doi.org/10.1016/j.ymssp.2011.02.005.
Xiong, K., Zhang, H.Y. and Chan, C.W. (2006), "Performance evaluation of UKF-based nonlinear filtering", *Automatica*, **42**(2), 261-270. https://doi.org/10.1016/j.automatica.2005.10.004.
Xu, L.H., Fan, X.W. and Li, Z.X. (2016), "Development and experimental verification of a pre-pressed spring self-centering energy dissipation brace", *Eng. Struct.*, **127**, 49-61. https://doi.org/10.1016/j.engstruct.2016.08.043.
Xu, L.H., Fan, X.W. and Li, Z.X. (2017), "Cyclic behavior and failure mechanism of self-centering energy dissipation braces with pre-pressed combination disc springs", *Earthq. Eng. Struct. Dynam.*, **46**(7), 1065-1080. https://doi.org/10.1002/eqe.2844.
Zhou, Z., Xie, Q., Lei, X., He, X. and Meng, S. (2015), "Experimental investigation of the hysteretic performance of dual-tube self-centering buckling-restrained braces with composite tendons", *J. Compos. Construct.*, **19**(6), https://doi.org/10.1061/(ASCE)CC.1943-5614.0000565.
Zhou, Z., Xie, Q., Lei, X.C., He, X.T. and Meng, S.P. (2015), "Experimental investigation of the hysteretic performance of dual-tube self-centering buckling-restrained braces with composite tendons", *J. Compos. Construct.*, **19**(6), https://doi.org/10.1061/(ASCE)CC.1943-5614.0000565.
Zhu, S. and Zhang, Y. (2008), "Seismic analysis of concentrically braced frame systems with self-centering friction damping braces", *J. Struct. Eng.*, **134**(1), 121-131. https://doi.org/10.1061/(ASCE)0733-9445(2008)134:1(121).
Zhu, S.Y. and Zhang, Y.F. (2007), "Seismic behaviour of self-centring braced frame buildings with reusable hysteretic damping brace", *Earthq. Eng. Struct. Dynam.*, **36**(10), 1329-1346. https://doi.org/10.1002/eqe.683.
Zhu, S.Y. and Zhang, Y.F. (2008), "Seismic analysis of concentrically braced frame systems with self-centering friction damping braces", *J. Struct. Eng.*, **134**(1), 121-131. https://doi.org/10.1061/(ASCE)0733-9445(2008)134:1(121).

CC

Notations

m	System mass
u	System displacement
t	Time
F	Restoring force
c	Viscous damping
z	Hysteretic displacement
k	Stiffness
α	Ratio of yield and initial tangent stiffness
β γ	Parameter of controlling the loop size
A	Parameter of the tangent stiffness
n	Parameter of controlling the loop smoothness
δ_η	Parameter of stiffness degradation
δ_v	Parameter of strength degradation
ε	Hysteretic energy
Sgn()	Signum function
$h(z,\varepsilon)$	Pinching function
q	Parameter of pinching level
p	Parameter of the rate of initial drop in slope
ζ_s	Parameter of total slip
ψ	Parameter of contribution to amount of pinching
δ_ψ	Parameter of the rate of pinching spread
λ	Parameter of the pinching ratio
f_0	Pre-stressing force of the self-centering system
u_g	Excitation